



HAL
open science

Electrical transport properties of black phosphorus based field-effect transistor with Au/Co/MgO tunneling contacts

Shiheng Liang, Huaiwen Yang, Abdelhak Djeflal, Bingshan Tao, Stefan Mc-Murtry, Stéphane Mangin, Yuan Lu

► To cite this version:

Shiheng Liang, Huaiwen Yang, Abdelhak Djeflal, Bingshan Tao, Stefan Mc-Murtry, et al.. Electrical transport properties of black phosphorus based field-effect transistor with Au/Co/MgO tunneling contacts. *Journal of Applied Physics*, 2017, 122 (16), pp.164301. 10.1063/1.5000524 . hal-02011640v1

HAL Id: hal-02011640


<https://hal.univ-lorraine.fr/hal-02011640v1>

Submitted on 8 Feb 2019 (v1), last revised 8 Feb 2019 (v2)

HAL is a multi-disciplinary open access archive for the deposit and dissemination of scientific research documents, whether they are published or not. The documents may come from teaching and research institutions in France or abroad, or from public or private research centers.

L'archive ouverte pluridisciplinaire **HAL**, est destinée au dépôt et à la diffusion de documents scientifiques de niveau recherche, publiés ou non, émanant des établissements d'enseignement et de recherche français ou étrangers, des laboratoires publics ou privés.

AUTHOR QUERY FORM

	Journal: J. Appl. Phys.	Please provide your responses and any corrections by annotating this PDF and uploading it according to the instructions provided in the proof notification email.
	Article Number: 049740JAP	

Dear Author,

Below are the queries associated with your article; please answer all of these queries before sending the proof back to AIP.

Article checklist: In order to ensure greater accuracy, please check the following and make all necessary corrections before returning your proof.

1. Is the title of your article accurate and spelled correctly?
2. Please check affiliations including spelling, completeness, and correct linking to authors.
3. Did you remember to include acknowledgment of funding, if required, and is it accurate?

Location in article	Query / Remark: click on the Q link to navigate to the appropriate spot in the proof. There, insert your comments as a PDF annotation.
AQ1	Please check that the author names are in the proper order and spelled correctly. Also, please ensure that each author's given and surnames have been correctly identified (given names are highlighted in red and surnames appear in blue).
AQ2	Please provide volume and page number for Ref. 22.
AQ3	We were unable to locate a digital object identifier (doi) for Ref(s). 20 and 22. Please verify and correct author names and journal details (journal title, volume number, page number, and year) as needed and provide the doi. If a doi is not available, no other information is needed from you. For additional information on doi's, please select this link: http://www.doi.org/ .

Thank you for your assistance.

1 Electrical transport properties of black phosphorus based field-effect 2 transistor with Au/Co/MgO tunneling contacts

3 Shiheng Liang, Huaiwen Yang, Abdelhak Djeflal, Bingshan Tao, Stefan Mc-Murtry,
4 Stéphane Mangin, and Yuan Lu^{a)}

5 Institut Jean Lamour, UMR 7198, CNRS-Université de Lorraine, BP 239, 54506 Vandœuvre, France

6 (Received 16 August 2017; accepted 10 October 2017; published online xx xx xxxx)

7 Black phosphorus (BP) has recently emerged as a promising two-dimensional direct bandgap semi-
8 conducting material. Here, we report the fabrication and the electrical transport measurements of
9 the black phosphorus based field-effect transistor with the Au/Co/MgO as drain and source tunnel-
10 ing contacts. By modulating the back-gate voltage, the multilayer black phosphorus channel exhib-
11 its ambipolar characteristics (both *n*-type and *p*-type) and the conduction behavior can be switched
12 from hole dominated to electron dominated transport region. In the hole dominated region, we have
13 measured a minimum of Schottky barrier height of 37 meV for Au/Co/MgO contact on BP.
14 Moreover, the transistor ON/OFF (I_{on}/I_{off}) ratio is obtained as large as 10^7 at 20 K and 10^5
15 at 300 K. A systematic study of the temperature and the back-gate voltage dependent conduction
16 properties has been performed to understand the modulation of band structure and the ambipolar
17 behavior. The demonstration of high ON/OFF ratio and low Schottky barrier height by using
18 Au/Co/MgO tunneling contacts reveals a promising potential for spintronics applications with mul-
19 tilayer black phosphorus field-effect transistor. *Published by AIP Publishing.*

<https://doi.org/10.1063/1.5000524>

20 I. INTRODUCTION

21 Two-dimensional (2D) materials with atomic thickness
22 have been recently unveiled as an important family of materi-
23 als in physics and materials science.¹⁻⁹ Since the discovery of
24 graphene in 2004,¹ a fair amount of research has been dedi-
25 cated to fabricate other thin layer 2D materials, for examples
26 of boron nitride¹⁰ and transition metal dichalcogenides
27 (TMDs) materials.³⁻⁹ The understanding of physics and mater-
28 ial characteristics of 2D materials leads to the possibility of
29 many applications, such as transistors,^{7,9} optoelectronics,¹¹
30 sensors,¹² photovoltaics,¹³ medicine,¹⁴ and energy storage.¹⁵
31 In the 2D material family, graphene is known as a semicon-
32 ductor with zero bandgap. Despite its high mobility, the gra-
33 phene is not suitable to be used as field-effect transistors
34 (FETs)^{1,2} due to the zero bandgap. Another 2D material is
35 boron nitride, which is an insulator and can be used as a tun-
36 nel barrier in 2D-heterostructure device to improve the phys-
37 ical properties.¹⁰ Besides the above two types of 2D materials,
38 TMDs such as MoS₂, WSe₂, and MoSe₂ have semiconducting
39 properties and can play the role of drain-source channel in
40 FETs, but their mobility is relatively low.³⁻⁹

41 Recently, black phosphorus (BP) has attracted a large
42 amount of attention and emerged as an important 2D mate-
43 rial due to its interesting physics properties.¹⁶⁻²⁴ The BP has
44 a layer stacked structure by van der Waals interactions. The
45 monolayer (ML) BP has a direct bandgap of about 2 eV. For
46 multilayer BP, the band gap decreases with the increase of
47 number of layers, changing from 2 eV (ML) to about 0.3 eV
48 (bulk). This provides a wide range of tunability of bandgap
49 for the multilayer BP.¹⁶ In addition, BP has a larger carrier

mobility (highest values up to $\sim 1000 \text{ cm}^2 \text{ V}^{-1} \text{ s}^{-1}$ at room 50
temperature)¹⁸ compared to TMDs, which is better to serve 51
as channel for FET applications. Moreover, by using BP as 52
channel, the FET with ambipolar modulated behavior (both 53
n-type and *p*-type) can be realized.¹⁷⁻²¹ Recently, spin trans- 54
port experiments have also been demonstrated in ultrathin 55
multilayer BP based non-local spin valve structures.²² A 56
long spin diffusion length ($> 2.5 \mu\text{m}$) was measured owing to 57
the high mobility and low spin-orbit coupling properties of 58
BP. Therefore, great efforts have been carried out to push the 59
BP based devices towards application in nano-electron- 60
ics,^{17,19} optoelectronics,^{20,21} FETs,¹⁸ and spintronics.²² 61

62 In this work, we have fabricated the BP based FETs
63 with Au/Co/MgO tunneling contacts and systematically stud-
64 ied the transport properties as a function of back-gate voltage
65 and temperature. The ambipolar characteristics (both *n*-type
66 and *p*-type) in multilayer BP has been observed with a high
67 ON/OFF ratio as large as 10^7 . The Schottky barrier height is
68 measured as low as 37 meV for Au/Co/MgO contact on BP.
69 The high ON/OFF ratio and low Schottky barrier height
70 demonstrate that BP has a promising potential for future
71 FET and spintronics applications.

72 II. EXPERIMENT

73 Figure 1(a) shows the optical image of our BP based
74 FET device. First, a flake of multilayer BP was mechanically
75 exfoliated onto a Si(n^{++})/SiO₂(280 nm) substrate as the FET
76 channel. The thickness of this flake was measured by an
77 atomic force microscopy (AFM) to be about 7 nm [inset of
78 Fig. 1(a)]. Considering 0.5 nm for one ML BP,¹⁸ the thick-
79 ness of the flake corresponds to about 14 MLs. Second,
80 e-beam lithography (Raith-150) was performed to define five

^{a)}Email: yuan.lu@univ-lorraine.fr

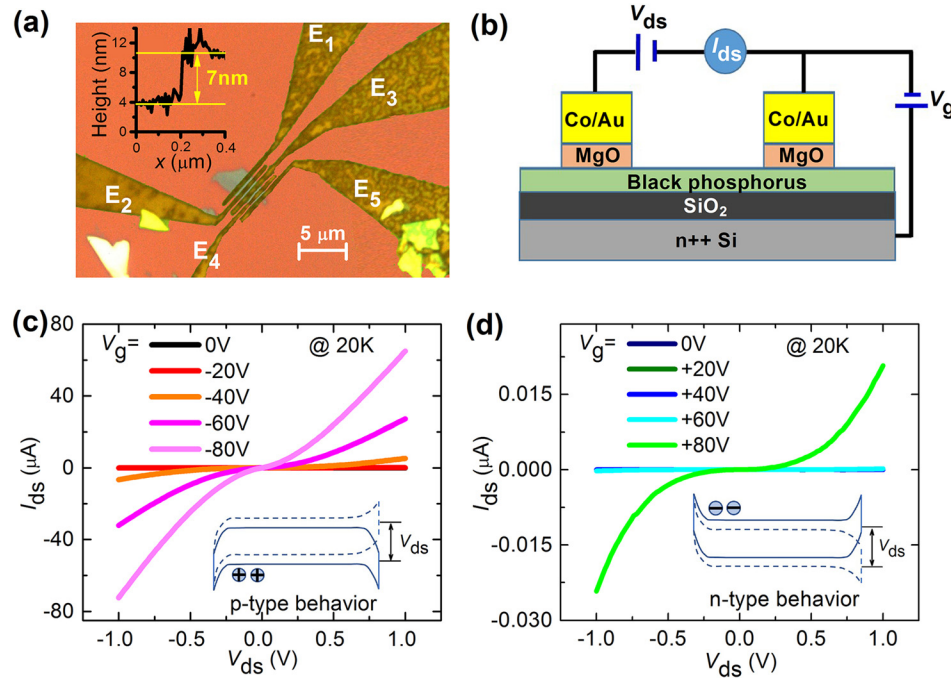


FIG. 1. (a) Optical image of black phosphorus flake exfoliated on $\text{Si}(n^{++})/280 \text{ nm SiO}_2$ substrate with contacts of $\text{Au}(10 \text{ nm})/\text{Co}(10 \text{ nm})/\text{MgO}(2 \text{ nm})$. Inset: the thickness of this BP flake was measured by AFM to be about 7 nm. (b) Schematics of BP based field effect transistor. A drain-source bias (V_{ds}) was applied to inject the current I_{ds} through the BP channel. Meanwhile, a back-gate voltage (V_g) was applied between the substrate and one contact to modulate the carrier density in the BP channel. (c) Output characteristics of drain-source current-voltage ($I_{ds}-V_{ds}$) measured with applying negative back-gate voltages V_g . Inset: schematic of band profile in BP by applying V_{ds} under negative V_g . (d) Output characteristics of drain-source current-voltage ($I_{ds}-V_{ds}$) measured with applying positive back-gate voltages V_g . Inset: schematic of band profile in BP by applying V_{ds} under positive V_g .

81 electrodes with a width of 500 nm on the selected flake. The
 82 distance between each electrode is about 450 nm. Then the
 83 sample was introduced into a molecular beam epitaxy
 84 (MBE) system to deposit the ferromagnetic (FM) electrodes
 85 as drain and source tunneling contacts, which consists of
 86 $\text{Au}(10 \text{ nm})/\text{Co}(10 \text{ nm})/\text{MgO}(2 \text{ nm})$. The 2 nm MgO is used
 87 as a tunnel barrier between metals and BP to effectively
 88 reduce the contact Schottky barrier height.²⁵ After deposition
 89 and lift-off procedures, a second e-beam lithography was
 90 performed to define the large pads for electrical connection.
 91 $\text{Au}(190 \text{ nm})/\text{Ti}(10 \text{ nm})$ was thermally evaporated in a
 92 PLASSYS MEB400s system for the large pads. Finally, the
 93 device was annealed at 120°C for one hour in vacuum and
 94 then followed by the coverage of 10 nm MgO protection
 95 layer. Figure 1(b) shows the schematic of electric character-
 96 ization of BP based transistor. A drain-source bias (V_{ds}) was
 97 applied between the two contacts to inject the current I_{ds}
 98 through the BP channel. Meanwhile, a back-gate voltage
 99 (V_g) was applied between the substrate and one electrode to
 100 modulate the carrier density in the BP channel.

101 III. RESULTS AND DISCUSSIONS

102 A. Drain-source current-voltage ($I_{ds}-V_{ds}$) 103 characteristics

104 The two-terminal drain-source current-voltage charac-
 105 teristics ($I_{ds}-V_{ds}$) were studied at 20 K between the electro-
 106 des E1 and E2 with negative and positive back-gate voltages
 107 [Figs. 1(c) and 1(d), respectively]. From the measurement of
 108 $I_{ds}-V_{ds}$, the back-gate voltages show an efficient modulation
 109 on the I_{ds} , which indicates the field-effect transistor behavior.
 110 At $V_g = 0 \text{ V}$, the current density is rather low ($I_{ds} < 1 \text{ pA}$ at
 111 $V_{ds} = \pm 1 \text{ V}$). As soon as we applied a negative or positive
 112 back-gate voltage V_g , the $I_{ds}-V_{ds}$ characteristics dramatically
 113 change. The quasi-symmetric nonlinearity of $I_{ds}-V_{ds}$ is
 114 attributed to the back-to-back Schottky diode structures of

the device, which is induced by the Schottky contacts of Co/
 MgO on BP [inset of Figs. 1(c) and 1(d)]. It is found that
 applying negative V_g can get much higher current density
 than that with positive V_g . Under a negative back-gate volt-
 age of $V_g = -80 \text{ V}$, I_{ds} can reach $80 \mu\text{A}$ at $V_{ds} = \pm 1 \text{ V}$, while
 there is about $0.02 \mu\text{A}$ at $V_{ds} = \pm 1 \text{ V}$ under a positive back-gate
 voltage of $V_g = +80 \text{ V}$. In fact, at different V_g , the trans-
 port mechanism is different since V_g can effectively modu-
 late the Fermi level (E_F) inside the bandgap of BP. Under the
 negative back-gate voltage, the E_F is attracted to be close to
 the energy of valence band maximum (E_V) of BP, resulting
 in the hole conduction transport. However, under positive
 back-gate voltage, the E_F is pushed close to the energy of
 conduction band minimum (E_C) of BP, resulting in the elec-
 tron conduction transport. The larger conductivity for hole
 transport region indicates a higher carrier density in BP for
 hole transport, which means that the E_F in our BP covered
 with MgO should be much closer to E_V than E_C at zero V_g .

133 B. Field-effect transistor ($I_{ds}-V_g$) characteristics

134 The field-effect transistor characteristics were measured
 135 from the I_{ds} vs. V_g curves at different temperature, as shown
 136 in Fig. 2(a). The asymmetric ambipolar behavior can be
 137 observed in all investigated temperature region. At large
 138 negative back-gate voltage ($V_g = -80 \text{ V}$) when hole trans-
 139 port is dominated, the temperature dependence is not evident
 140 with $V_{ds} = -1 \text{ V}$. However, at a large positive back-gate volt-
 141 age ($V_g = +80 \text{ V}$) when electron transport is dominated, the
 142 conductance with $V_{ds} = -1 \text{ V}$ can be changed more than one
 143 order from 20 K to 300 K. Since the variation of mobility
 144 with temperature is small with $V_{ds} = -1 \text{ V}$ (see below), the
 145 different temperature dependent conductance mainly reflects
 146 different carrier densities in the p -type and n -type transport
 147 region. If assuming that the carrier density in BP follows the
 148 thermal activation rule in the intrinsic semiconductor, the

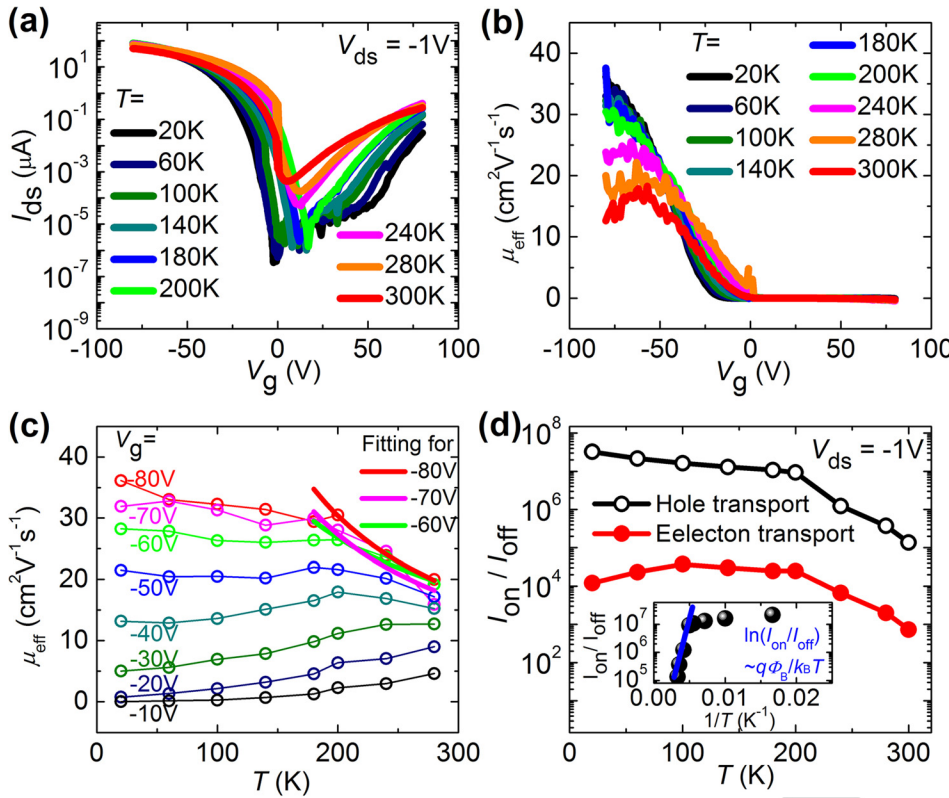


FIG. 2. (a) Transfer characteristics of $I_{ds} - V_g$ in logarithmic scale measured with $V_{ds} = -1\text{V}$ at different temperatures. (b) Extracted effective mobility μ_{eff} versus V_g at different temperatures with $V_{ds} = -1\text{V}$. (c) Temperature dependent mobility μ_{eff} measured under different back-gate voltages V_g . (d) Temperature dependent $I_{\text{on}}/I_{\text{off}}$ ratio measured for hole transport (black open) and electron transport (red solid) situations, respectively. Inset: $I_{\text{on}}/I_{\text{off}}$ ratio under hole transport in logarithmic scale plotted with $1/T$. The blue line is a linear fitting for $\ln(I_{\text{on}}/I_{\text{off}})$ vs. $1/T$.

149 hole and electron densities can be expressed by $p = n_i e^{\frac{E_i - E_F}{k_B T}}$
 150 and $n = n_i e^{\frac{E_F - E_i}{k_B T}}$, respectively.²⁶ $n_i = 2.509 \times 10^{19} \left(\frac{m_n m_p}{m_0^2}\right)^{3/4}$
 151 $\left(\frac{T}{300}\right)^{3/2} e^{-\frac{E_g}{2k_B T}}$ (cm^{-3}) is the intrinsic carrier density, and E_i is
 152 the intrinsic Fermi energy. m_n , m_p , and, m_0 are the electron
 153 mass in E_C , the hole mass in E_V , and the free electron mass,
 154 respectively. This can easily explain that the larger $|E_i - E_F|$
 155 results in higher carrier density when increasing V_g . In addition,
 156 the ratio of carrier density between 300 and 20 K can
 157 be expressed as $p(300\text{K})/p(20\text{K}) = \left(\frac{300}{20}\right)^{3/2} e^{\frac{E_i - E_F - 0.5E_g}{k_B} \left(\frac{1}{300} - \frac{1}{20}\right)}$
 158 $\propto e^{\frac{0.5E_g - (E_i - E_F)}{k_B}}$ for hole transport region and
 159 $n(300\text{K})/n(20\text{K}) = \left(\frac{300}{20}\right)^{3/2} e^{\frac{E_F - E_i - 0.5E_g}{k_B} \left(\frac{1}{300} - \frac{1}{20}\right)}$ $\propto e^{\frac{0.5E_g - (E_F - E_i)}{k_B}}$ for
 160 electron transport region. This explains that the carrier den-
 161 sity is more sensitive to the temperature variation when
 162 $|E_i - E_F|$ is smaller under positive V_g in the n -type transport
 163 region.

164 C. Temperature dependent channel mobility

165 The effective field-effect mobility can be extracted from
 166 the slope of dI_{ds}/dV_g from the $I_{ds} - V_g$ curves, as shown in
 167 Fig. 2(b)

$$\mu_{\text{eff}} = \frac{dI_{ds}}{dV_g} \frac{L}{wC_i V_{ds}} \quad (1)$$

168 where L is the length of the channel (450 nm), w is the width
 169 of the channel (2.9 μm), and C_i is the gate capacitance
 170 [$1.3 \times 10^{-4} \text{Fm}^{-2}$ for Si/SiO₂(280 nm) substrate]. The effec-
 171 tive field-effect mobility is found to increase under negative
 172 V_g [Fig. 2(c)]. At 20 K, with $V_{ds} = -1\text{V}$ and $V_g = -80\text{V}$, we

can obtain a mobility of $\mu_{\text{eff}} \sim 38 \text{cm}^2 \text{V}^{-1} \text{s}^{-1}$. This value is
 lower than the previously reported values, which could be due
 to the scattering related to the charged impurities at BP/sub-
 strate interface at low temperature.²² The enhancement of
 mobility with the increase of V_g as well as the carrier den-
 sity is due to the shielding effect of carrier to the Coulomb scatter-
 ing from the charged impurities,²⁶ which has also been
 observed in MoS₂ based FET system.⁹ Figure 2(c) displays
 the variation of μ_{eff} with temperature measured under different
 V_g . It is interesting to find that there exist two distinct tempera-
 ture dependences. μ_{eff} decreases with the increasing T when
 $V_g < -50\text{V}$, while it increases with T when $V_g > -50\text{V}$. For
 $V_g < -50\text{V}$, μ_{eff} decreases faster when $T > 200\text{K}$, which is
 due to the carrier-phonon scattering at higher temperature.²⁷
 This can be expressed as $\mu \sim T^{-\alpha}$, the exponent α is fitted to
 be 1.27 and 1.21, and 0.91 for the data at $V_g = -60\text{V}$, -70V
 and -80V , respectively. For atomically thin 2D materials, the
 exponent α is reported to be ~ 1.69 for MoS₂,²⁷ and between 1
 and 6 for graphene.²⁸⁻³⁰ Below 200 K, the slower decrease of
 μ suggests an impurity-dominated scattering mechanism.¹⁸
 For $V_g > -50\text{V}$ when E_F moves far away from E_V , μ
 increases monotonically with the increase of T . This behavior
 means that when the carrier density is very low, the mobility
 is only limited by the scattering from the charged impurities.²⁶

D. Temperature dependent transistor ON/OFF ratio

The transistor current ON/OFF ratio can be extracted
 from $I_{\text{on}} (|V_g| = 80\text{V})/I_{\text{off}} (V_g = 0\text{V})$ from the $I_{ds} - V_g$ curves.
 At 20 K, a large ON/OFF ratio of 10^7 is obtained for hole
 transport and a ratio of 10^4 is measured for electron trans-
 port. The ON/OFF ratio for hole transport is found to be
 much larger than the recent reported values: 10^3 with Au/BP

204 contacts,²¹ 10^5 with Au/Pd/Ti/BP contacts,²⁰ and 10^6 with
 205 Co/TiO₂/BP contacts.²⁴ This high I_{on}/I_{off} ratio provides prom-
 206 ising device characteristics for future applications. Figure 2(d)
 207 shows the temperature dependent I_{on}/I_{off} behavior. For the
 208 holes dominated FET, the I_{on}/I_{off} increases with the decrease
 209 of temperature. Since I_{on} has little change with temperature,
 210 the improvement of I_{on}/I_{off} at low temperature is mainly
 211 attributed to the reduction in I_{off} current. When $T > 200$ K, the
 212 I_{off} current (at $V_g \sim 0$ V) is mainly dominated by the therm-
 213 ionic injection through Schottky barrier, which is proportional
 214 to $\exp(-q\Phi_B/k_B T)$,³¹ where k_B is the Boltzmann constant and
 215 Φ_B is Schottky barrier height [see also below for Eq. (2)].
 216 Thus, the slope of $-q\Phi_B/k_B$ can be extracted from a linear fit-
 217 ting of $\ln(I_{on}/I_{off})$ versus $1/T$, as shown in the insert of Fig.
 218 2(d). The slope obtained from 300 K to 200 K leads to a
 219 Schottky barrier height Φ_B of 270 meV at $V_g = 0$ V.
 220 Moreover, both for hole and electron transport regions, the
 221 I_{on}/I_{off} do not improve too much when the temperature is
 222 below 200 K. This could be due to the presence of tunneling
 223 through defect states inside the MgO tunnel barrier.³² This
 224 phenomenon has also been observed in both carbon nano-
 225 tube³³ and graphene nanoribbon transistors.³⁴

226 **E. Determination of Schottky barrier height**

227 In order to extract the Schottky barrier height (Φ_B) of
 228 Au/Co/MgO contact on BP [inset of Fig. 3(a)] and under-
 229 stand the effect of V_g on Φ_B , we have measured the $I_{ds}-V_{ds}$
 230 characteristics with different V_g from 140 K to 200 K [Fig.
 231 3(a)]. In this temperature range, the thermionic emission
 232 transport mechanism through the Schottky barrier can be
 233 mainly considered. We have employed a two-dimensional

thermionic emission equation describing the electrical trans- 234
 port through the Schottky barrier into the BP channel³⁵ 235

$$I_{ds} = AA^*T^{1.5} \exp \left[-\frac{q}{k_B T} \left(\Phi_B - \frac{V_{ds}}{n_0} \right) \right] \quad (2)$$

where A is the contact area, A^* is the Richardson constant, q is 236
 the hole charge, and n_0 is the ideality factor. Figure 3(b) shows 237
 the Arrhenius plot [$\ln(I_{ds}/T^{3/2})$ vs. $1000/T$] for different V_{ds} . 238
 The slopes $S(V_{ds})$ extracted from the Arrhenius plot follow a linear 239
 dependence with V_{ds} : $S(V_{ds}) = -(q/1000k_B)(\Phi_B - V_{ds}/n_0)$, as 240
 displayed in Fig. 3(c). Then the Schottky barrier height can 241
 be evaluated from the extrapolated value at zero V_{ds} [S_0 242
 $= -(q\Phi_B/1000k_B)$]. A similar procedure has been used to 243
 determine Φ_B with different V_g , as shown in Fig. 3(d). 244

As shown in the inset of Fig. 3(d), the back-gate mainly 245
 plays two roles. One is to modulate the Fermi level inside 246
 the BP bandgap yielding a change of the carrier density in 247
 the channel. The second role is to modify the Schottky barrier 248
 profile and depletion layer width. In Fig. 3(d), we can 249
 identify two regions from the variation of Φ_B vs. V_g . For 250
 $V_g > -15$ V when the depletion layer is thick, the thermionic 251
 emission dominates, and this results in a large linear increase 252
 of Φ_B at low $|V_g|$. Note here, the Φ_B obtained at $V_g = 0$ V is 253
 ~ 200 meV, which is in good agreement with the value of 254
 270 meV estimated from I_{on}/I_{off} ratio at $V_g = 0$ V. For 255
 $V_g < -15$ V, the tunneling current through the thin Schottky 256
 barrier impinges on the linearity of Φ_B . The real value of Φ_B 257
 for Co/MgO on BP is obtained at the point of the onset of the 258
 deviation ($V_f = -15$ V) equaling thus 37 meV, which is cor- 259
 responding to the flat band condition. This Φ_B value is much 260
 smaller than the recent reports of Py contacts ($110-200$ meV),³⁶ 261
 Au/Ti/BP contacts (200 meV),¹⁸ and Co/TiO₂/contacts 262

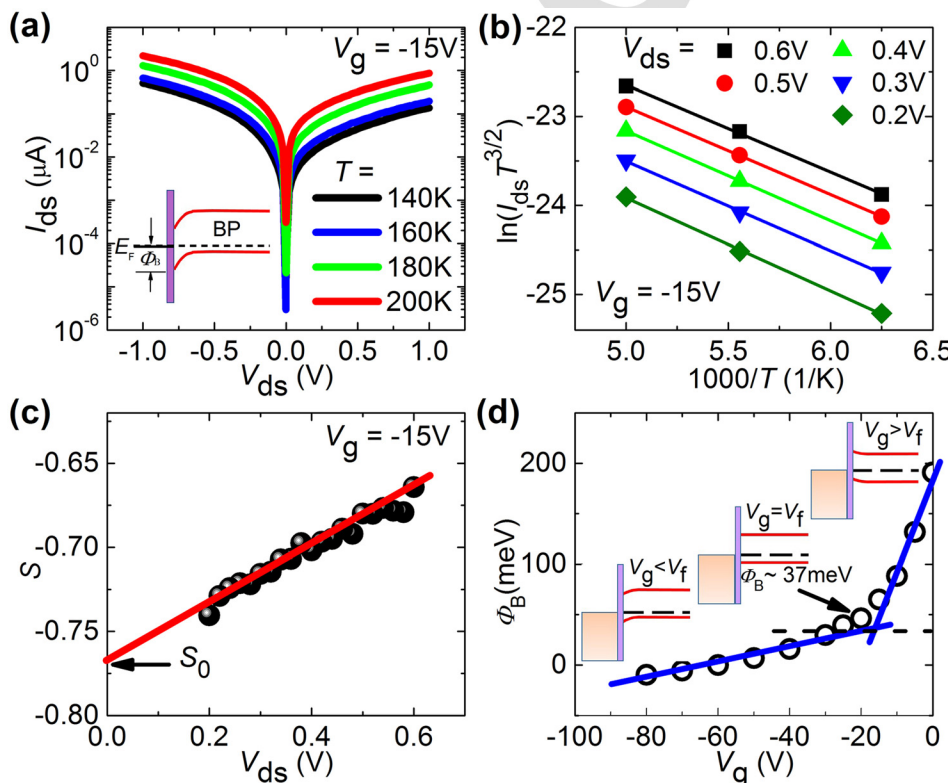


FIG. 3. (a) $I_{ds} - V_{ds}$ characteristics for temperatures between 140 and 200 K under $V_g = -15$ V. Inset: Schematics of the Schottky barrier height for Co/MgO contact on *p*-type BP. (b) $\ln(I_{ds}/T^{3/2})$ versus $1000/T$ at different drain-source bias (V_{ds}), in an Arrhenius plot with linear fits in the temperature range from 160 K to 200 K. (c) Bias dependence of the slope (S) from linear fits. The slope at zero V_{ds} (S_0) is used to extract the Schottky barrier height Φ_B . (d) Schottky barrier height Φ_B extracted at different back-gate voltages. The real Φ_B (37 meV) for Au/Co/MgO on BP is obtained with the flat band condition ($V_g = V_f = -15$ V), which is defined at the cross point from the linear response of Φ_B with V_g (blue solid lines). Inset: band diagram of Co/MgO/BP interfaces with different back-gate voltages.

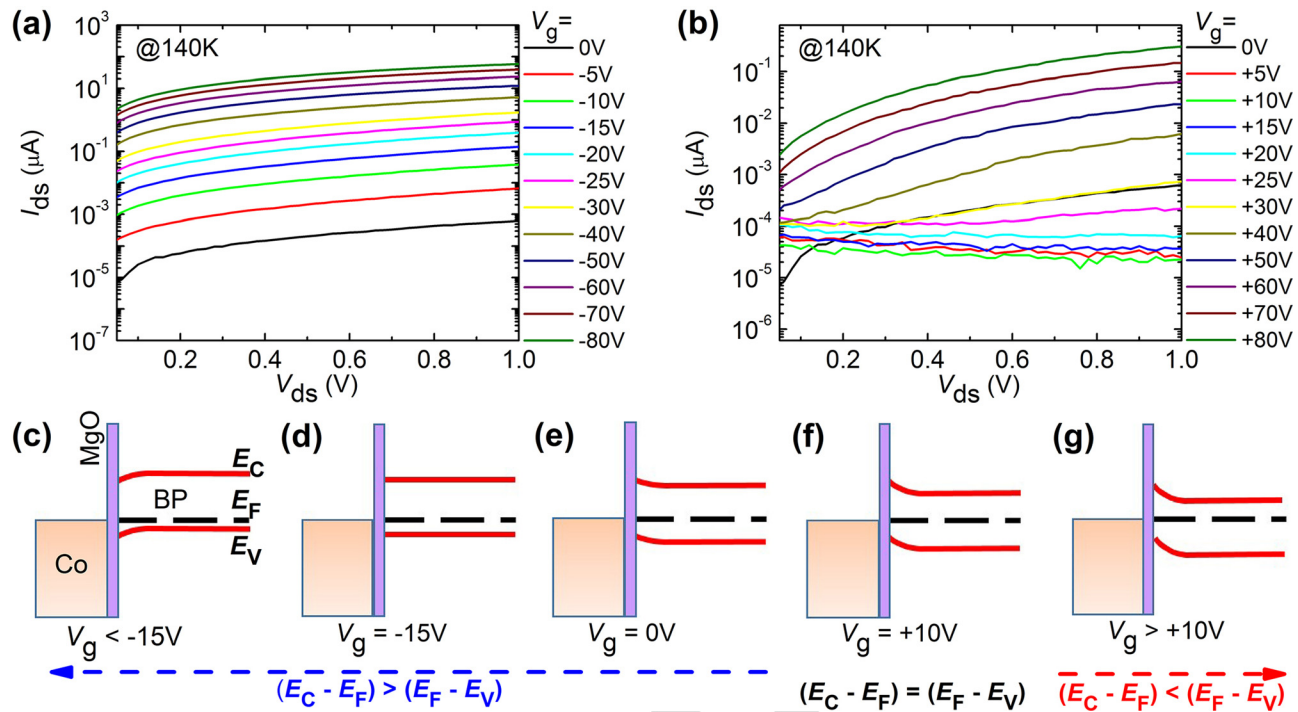


FIG. 4. Characteristics of $I_{ds} - V_{ds}$ at 140 K, measured under (a) different negative back-gate voltages and (b) different positive back-gate voltages. (c)–(g) Band structure of Co/MgO/BP interface modulated under different back-gate voltages. (c) $V_g < -15$ V; (d) $V_g = -15$ V; (e) $V_g = 0$ V; (f) $V_g = +10$ V; (g) $V_g > +10$ V.

(50 meV).²⁴ The efficient lowering Φ_B by inserting thin tunnel barrier between the ferromagnetic metal and 2D materials have also been reported in TMDs systems.^{25,37,38} This result of low Schottky barrier by using Au/Co/MgO tunneling contact is important for future application of BP based FET and spintronics.

F. Modulation of band structure by back-gate voltage

In the end, to have a global view of the band structure modulation by the back-gate voltage, we have measured I_{ds} vs. V_{ds} with applying different V_g at 140 K. Figures 4(a) and 4(b) show $I_{ds} - V_{ds}$ characteristics with negative and positive V_g , respectively. From the analysis of Φ_B vs. V_g , we have identified that the flat band condition reaches at $V_g = -15$ V [Fig. 3(d)]. In addition, due to the hole transport feature, the band structure can be schematically drawn as in Fig. 4(d) with a situation of $E_C - E_F > E_F - E_V$. For $V_g < -15$ V, the depletion layer tilts the band down due to the E_F pinning at the interface [Fig. 4(c)]. With the increase of negative V_g , more hole can be injected into BP by crossing the depletion layer. For $V_g > -15$ V, the depletion layer tilts the band up at the interface. However, it is not the case that the larger V_g results in larger I_{ds} . From Fig. 4(b), we can see that when we increase V_g from 0 to +80 V, the I_{ds} firstly decreases to a minimum at $V_g = +10$ V and then increases with V_g . This indicates that it is hard to inject both holes and electrons at $V_g = +10$ V, which should correspond to the condition that E_F is located in the middle of band ($E_C - E_F = E_F - E_V$), as shown in Fig. 4(f). When continuing with the increasing V_g , both the E_F moving closer to E_C and the width of depletion region becoming thinner make the conditions favorable for the electron injection into the BP

conduction band [Fig. 4(g)]. Finally, at zero back-gate voltage, the BP shows a hole transport behavior ($E_C - E_F > E_F - E_V$), while the depletion layer tilts up [Fig. 4(e)]. This could be related to the defects in the contact regions, which effectively pin the Fermi level at MgO/BP interface.

IV. CONCLUSION

In summary, we have studied the electrical transport properties in multilayer BP based FET device with Au/Co/MgO tunneling contacts. In the hole dominated transport region, we have measured a minimum of Schottky barrier height of 37 meV for Au/Co/MgO contact on BP. Moreover, the transistor ON/OFF (I_{on}/I_{off}) ratio is obtained as large as 10^7 at 20 K and 10^5 at 300 K. A systematic study of the temperature and back-gate voltage dependent conduction measurements has been performed to understand the modulation of the band structure and the ambipolar behavior. This demonstration of high ON/OFF ratio and low Schottky barrier height by using Au/Co/MgO tunneling contacts reveal a great potential promising for spintronics applications with multilayer black phosphorus field effect transistor.

ACKNOWLEDGMENTS

This work was supported by the French National Research Agency (ANR) MoS2ValleyControl project (Grant No. ANR-14-CE26-0017-04) and the joint ANR-National Natural Science Foundation of China (NNSFC) ENSEMBLE project (Grant Nos. ANR-14-CE26-0028-01 and NNSFC 61411136001). The experiments were performed using the equipment from the platform TUBE-Davm funded by FEDER (EU), ANR, the Region Lorraine, and Grand Nancy.

- 324 ¹S. Novoselov, A. K. Geim, S. V. Morozov, D. Jiang, Y. Zhang, S. V.
325 Dubonos, I. V. Grigorieva, and A. A. Firsov, "Electric field effect in atom-
326 ically thin carbon films," *Science* **306**, 666 (2004).
327 ²K. A. H. Castro Neto, F. Guinea, N. M. R. Peres, K. S. Novoselov, and A.
328 K. Geim, "The electronic properties of graphene," *Rev. Mod. Phys.* **81**,
329 109 (2009).
330 ³G. Fiori, F. Bonaccorso, G. Iannaccone, T. Palacios, D. Neumaier, A.
331 Seabaugh, S. K. Banerjee, and L. Colombo, "Electronics based on two-
332 dimensional materials," *Nat. Nanotechnol.* **9**, 768 (2014).
333 ⁴K. F. Mak, C. Lee, J. Hone, J. Shan, and T. F. Heinz, "Atomically thin MoS₂:
334 a new direct-gap semiconductor," *Phys. Rev. Lett.* **105**, 136805 (2010).
335 ⁵M. Xu, T. Liang, M. Shi, and H. Chen, "Graphene-like two-dimensional
336 materials," *Chem. Rev.* **113**, 3766 (2013).
337 ⁶D. Jariwala, V. K. Sangwan, L. J. Lauhon, T. J. Marks, and M. C. Hersam,
338 "Emerging device applications for semiconducting two-dimensional transi-
339 tion metal dichalcogenides," *ACS Nano* **8**, 1102 (2014).
340 ⁷B. Radisavljevic, A. Radenovic, J. Brivio, V. Giacometti, and A. Kis,
341 "Single-layer MoS₂ transistors," *Nat. Nanotechnol.* **6**, 147 (2011).
342 ⁸D. Xiao, G. Liu, W. Feng, X. Xu, and W. Yao, "Coupled spin and valley
343 physics in monolayers of MoS₂ and other group-VI dichalcogenides,"
344 *Phys. Rev. Lett.* **108**, 196802 (2012).
345 ⁹S. Liang, H. Yang, P. Renucci, B. Tao, P. Laczkowski, S. Mc-Murtry, G.
346 Wang, X. Marie, J. George, S. Petit-Watelot, A. Djéffal, S. Mangin, H.
347 Jaffres, and Y. Lu, "Electrical spin injection and detection in molybdenum
348 disulfide multilayer channel," *Nat. Commun.* **8**, 14947 (2017).
349 ¹⁰D. Pacilé, J. C. Meyer, Ç. Ö. Girit, and A. Zettl, "The two-dimensional
350 phase of boron nitride: Few-atomic-layer sheets and suspended mem-
351 branes," *Appl. Phys. Lett.* **92**, 133107 (2008).
352 ¹¹Q. H. Wang, K. Kalantar-Zadeh, A. Kis, J. N. Coleman, and M. S. Strano,
353 "Electronics and optoelectronics of two-dimensional transition metal
354 dichalcogenides," *Nat. Nanotechnol.* **7**, 699 (2012).
355 ¹²K. Lee, R. Gatensby, N. McEvoy, T. Hallam, and G. S. Duesberg, "High
356 performance sensors based on molybdenum disulfide thin films," *Adv.*
357 *Mater.* **25**, 6699 (2013).
358 ¹³M. Bernardi, M. Palummo, and J. C. Grossman, "Extraordinary sunlight
359 absorption and one nanometer thick photovoltaics using two-dimensional
360 monolayer materials," *Nano Lett.* **13**, 3664 (2013).
361 ¹⁴R. Kurapati, K. Kostarelos, M. Prato, and A. Bianco, "Biomedical uses for
362 2D materials beyond graphene: Current advances and challenges ahead,"
363 *Adv. Mater.* **28**, 6052 (2016).
364 ¹⁵X. Zhang, L. Hou, A. Ciesielski, and P. Samorì, "2D materials beyond gra-
365 phene for high-performance energy storage applications," *Adv. Energy*
366 *Mater.* **6**, 1600671 (2016).
367 ¹⁶V. Tran, R. Soklaski, Y. Liang, and L. Yang, "Layer-controlled band gap
368 and anisotropic excitons in few-layer black phosphorus," *Phys. Rev. B* **89**,
369 235319 (2014).
370 ¹⁷H. Liu, A. T. Neal, Z. Zhu, Z. Luo, X. Xu, D. Tománek, and P. D. Ye,
371 "Phosphorene: An unexplored 2D semiconductor with a high hole mobi-
372 lity," *ACS Nano* **8**, 4033 (2014).
373 ¹⁸L. Li, Y. Yu, G. Ye, Q. Ge, X. Ou, H. Wu, D. Feng, X. Chen, and Y.
374 Zhang, "Black phosphorus field-effect transistors," *Nat. Nanotechnol.* **9**,
375 372 (2014).
376 ¹⁹S. P. Koenig, R. A. Doganov, H. Schmidt, A. H. Castro Neto, and B.
377 Özyilmaz, "Electric field effect in ultrathin black phosphorus," *Appl.*
378 *Phys. Lett.* **104**, 103106 (2014).

379 ²⁰F. Xia, H. Wang, and Y. Jia, "Rediscovering black phosphorus as an aniso-
380 tropic layered material for optoelectronics and electronics," *Nat. Commun.*
381 **5**, 4458 (2014).
382 ²¹M. Buscema, D. J. Groenendijk, S. I. Blanter, G. A. Steele, H. S. J. van der
383 Zant, and A. Castellanos-Gomez, "Fast and broadband photoresponse of
384 few-layer black phosphorus field-effect transistors," *Nano Lett.* **14**, 3347
385 (2014).
386 ²²A. Avsar, J. Y. Tan, M. Kurpas, M. Gmitra, K. Watanabe, T. Taniguchi, J.
387 Fabian, and B. Özyilmaz, "Gate-tunable black phosphorus spin valve with
388 nanosecond spin lifetimes," *Nat. Phys.* **13**, 1000 (2017).
389 ²³Y. Du, H. Liu, Y. Deng, and P. D. Ye, "Device perspective for black phos-
390 phorus field-effect transistors: Contact resistance, ambipolar and scaling,"
391 *ACS Nano* **8**, 10035 (2014).
392 ²⁴M. V. Kamalakar, B. N. Madhushankar, A. Dankert, and S. P. Dash, "Low
393 Schottky barrier black phosphorus field-effect devices with ferromagnetic
394 tunnel contacts," *Small* **11**, 2209 (2015).
395 ²⁵J. Chen, P. M. Odenthal, A. G. Swartz, G. C. Floyd, H. Wen, K. Y. Luo,
396 and R. K. Kawakami, "Control of Schottky barriers in single layer MoS₂
397 transistors with ferromagnetic contacts," *Nano Lett.* **13**, 3106 (2013).
398 ²⁶S. M. Sze and K. K. Ng, *Physics of Semiconductor Devices* (Wiley, 2007).
399 ²⁷K. Kaasbjerg, K. S. Thygesen, and K. W. Jacobsen, "Phonon limited
400 mobility in n-type single-layer MoS₂ from first principles," *Phys. Rev. B*
401 **85**, 115317 (2012).
402 ²⁸E. H. Hwang and S. Das Sarma, "Acoustic phonon scattering limited car-
403 rier mobility in two-dimensional extrinsic graphene," *Phys. Rev. B* **77**,
404 115449 (2008).
405 ²⁹E. Mariani, A. J. Pearce, and F. von Oppen, "Fictitious gauge fields in
406 bilayer graphene," *Phys. Rev. B* **86**, 165448 (2012).
407 ³⁰H. Ochoa, E. V. Castro, M. I. Katsnelson, and F. Guinea, "Temperature-
408 dependent resistivity in bilayer graphene due to flexural phonons," *Phys.*
409 *Rev. B* **83**, 235416 (2011).
410 ³¹F. Xia, D. B. Farmer, Y. Lin, and P. Avouris, "Graphene field-effect tran-
411 sistors with high on/off current ratio and large transport band gap at room
412 temperature," *Nano Lett.* **10**, 715 (2010).
413 ³²Y. Lu, M. Tran, H. Jaffrès, P. Seneor, C. Deranlot, F. Petroff, J.-M.
414 George, B. Lépine, S. Ababou, and G. Jézéquel, "Spin-polarized inelastic
415 tunneling through insulating barriers," *Phys. Rev. Lett.* **102**, 176801
416 (2009).
417 ³³J. Appenzeller, M. Radosavljevic, J. Knoch, and P. Avouris, "Tunneling
418 versus thermionic emission in one-dimensional semiconductors," *Phys.*
419 *Rev. Lett.* **92**, 048301 (2004).
420 ³⁴Z. Chen, Y. M. Lin, M. J. Rooks, and P. Avouris, "Graphene nano-ribbon
421 electronics," *Physica E* **40**, 228 (2007).
422 ³⁵A. Anwar, B. Nabet, J. Culp, and F. Castro, "Effects of electron confine-
423 ment on thermionic emission current in a modulation doped hetero-
424 structure," *J. Appl. Phys.* **85**, 2663 (1999).
425 ³⁶Y. Anugrah, M. C. Robbins, P. A. Crowell, and S. J. Koester,
426 "Determination of the Schottky barrier height of ferromagnetic contacts to
427 few-layer phosphorene," *Appl. Phys. Lett.* **106**, 103108 (2015).
428 ³⁷W. Wang, Y. Liu, L. Tang, Y. Jin, T. Zhao, and F. Xiu, "Controllable
429 Schottky barriers between MoS₂ and permalloy," *Sci. Rep.* **4**, 6928
430 (2014).
431 ³⁸A. Dankert, L. Langouche, M. V. Kamalakar, and S. P. Dash, "High-per-
432 formance molybdenum disulfide field-effect transistors with spin tunnel
433 contacts," *ACS Nano* **8**, 476–482 (2014).

AQ3

AQ2